

Transport properties in gapped graphene through magnetic barrier in a laser field

Rachid El Aitouni,¹ Miloud Mekkaoui,¹ Ahmed Jellal,^{1,2,*} and Michael Schreiber³

¹*Laboratory of Theoretical Physics, Faculty of Sciences,
Chouaib Doukkali University, PO Box 20, 24000 El Jadida, Morocco*

²*Canadian Quantum Research Center, 204-3002 32 Ave Vernon, BC V1T 2L7, Canada*

³*Institut für Physik, Technische Universität, D-09107 Chemnitz, Germany*

We study the transport properties of Dirac fermions through gapped graphene through a magnetic barrier irradiated by a laser field oscillating in time. We use Floquet theory and the solution of Weber's differential equation to determine the energy spectrum corresponding to the three regions composing the system. The boundary conditions and the transfer matrix approach are employed to explicitly determine the transmission probabilities for multi-energy bands and the associated conductance. As an illustration, we focus only on the three first bands: the central band T_0 (zero photon exchange) and the two first side bands $T_{\pm 1}$ (photon emission or absorption). It is found that the laser field activates the process of translation through photon exchange. Furthermore, we show that varying the incident angle and energy gap strongly affects the transmission process. The conductance increases when the number of electrons that cross the barrier increases, namely when there is a significant transmission.

PACS numbers: 78.67.Wj, 05.40.-a, 05.60.-k, 72.80.Vp

KEYWORDS: Graphene, laser field, magnetic field, energy gap, transmission, Klein effect, conductance.

I. INTRODUCTION

Graphene is a two-dimensional carbon-based material that is one atom thick, and has atoms structured in a hexagonal shape like a honeycomb [1, 2]. Graphene possesses remarkable characteristics, including a very high mobility [3, 4], electrons moving with a speed 300 times lower than the speed of light, a good conductivity (minimal in the vicinity of the Dirac points, i.e., always the fermions pass), being flexible [5] and being very hard [6]. Due to these properties, graphene is becoming the most used material in the technological industries [7–9]. It is theoretically studied in the framework of the tight-binding model [10] and as a result, the energy spectrum shows a linear dispersion relation. In addition, the energy bands are in contact at six points [11, 12], called Dirac points K (K'), and form cones around them. It is surprising that electrons can pass from the valance band to the conduction band easily without any effect. This lack of excitation energy constitutes, in fact, an obstacle and a challenge for the fabrication of devices based on graphene. Consequently, to control the passage of electrons, an energy gap should be created between the two bands. Several studies have been reported on the subject to overcome such situations, for instance, either by deforming graphene to generate pseudo-magnetic fields that play the role of a real magnetic field [13, 14] or by stacking one layer of graphene on the other [15, 16].

On the other hand, fermions confined in graphene under barriers, at normal incidence, can cross them even if their energy is less than the barrier heights, an effect known as the Klein paradox [17]. For an oscillating potential over time, the energy spectrum acquires sub-bands, generating several transmission modes, and each mode corresponds to an energy band [18]. Furthermore, an applied magnetic field to graphene generates a quantized energy spectrum known as Landau levels [19–22]. Combining these with the oscillating potential gives rise to a current density in x - and y -directions [23]. When the graphene is irradiated by a time-varying laser field, subbands emerge in the energy spectrum, and then the barrier exchanges photons with the fermions, generating infinite transmission modes [18, 24–27]. As a consequence, the laser field suppresses the Klein effect, which makes it possible to control the passage of fermions.

We investigate how Dirac fermions can cross a gapped graphene subjected to a magnetic barrier and irradiated by a laser field. Within the framework of Floquet theory [28] and by using the solution of Weber's differential equation [29], we will be able to determine the eigenspinors corresponding to each region composing the system. These will be matched at boundaries and mapped in matrix form by applying the matrix transfer approach to finally get the transmission coefficients for all energy bands. Now, with the help of the current density, we derive the transmission probabilities for all modes. The conductance is also calculated by integrating the total transmission over all incident angles. Since it is not easy to treat all modes numerically, we limit our study to the first three bands, which are

* a.jellal@ucd.ac.ma

the central band ($l = 0$) and the two first side bands ($l = \pm 1$). We show that increasing the barrier width, or the incidence energy, decreases the transmissions, which implies that the number of electrons that cross the barrier decreases, consequently, the conductance decreases. On the other hand, when the intensity of the laser field increases, we observe that the transmissions decrease **but increase as long as the laser field frequency increases**. When the barrier width increases, it is found that the resonance peaks appear, and their number increases. Another set of results shows that the transmissions are almost zero when the incidence energy is less than the energy gap, and the Klein paradox is still present.

This paper is organized as follows. In Sec. II, we present the Hamiltonian describing our system and we solve the eigenvalue equations to determine the wave functions in the three regions. We use the boundary conditions and the matrix formalism to express the transmission probabilities of each band, and we calculate the integral of this total transmission which makes it possible to determine the conductance at zero temperature in Sec. III. We discuss our numerical results in Sec. IV. Finally, we conclude our work.

II. THEORETICAL MODEL

We study the behavior of Dirac fermions in a graphene sheet divided into three regions. Regions 1 and 3 contain only pristine graphene, whereas the gapped region 2 of width d is subjected to a perpendicular magnetic field and irradiated by a laser field, as shown in Fig. 1.

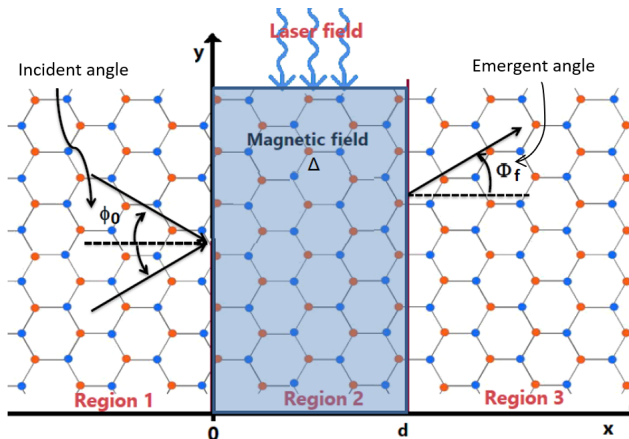


FIG. 1. Schematic presentation of a graphene sheet irradiated by a linearly polarized monochromatic laser field over a finite region of width d subjected to a mass term Δ and magnetic field.

The present system can be described the following Hamiltonian

$$H = v_F \vec{\sigma} \cdot \left[\vec{p} - \frac{e}{c} \left(\vec{A}_L(t) + \vec{A}_B(x) \right) \right] + \Delta \sigma_z \quad (1)$$

where $\sigma_{x,y,z}$ are Pauli matrices, $v_F \approx c/300$ is the Fermi velocity, $\vec{p} = -i\hbar \left(\frac{\partial}{\partial x}, \frac{\partial}{\partial y} \right)$ the momentum operator, e the electronic charge. The vector potential $\vec{A}_L(t)$ of the laser field in the dipole approximation [30] is generated by an electric field of amplitude F and frequency ω defined as $E(t) = F \sin(\omega t)$, which is given by

$$\vec{A}_L(x, y, t) = (0, A_0 \cos(\omega t), 0) \quad (2)$$

with the laser field amplitude $A_0 = \frac{F}{\omega}$. For the magnetic field, the vector potential $\vec{A}_B(x)$ is chosen in the Landau gauge $B(0, x, 0)$ and the continuity allows us to write

$$\vec{A}_B(x) = \begin{cases} 0, & x < 0 \\ Bx, & 0 < x < d \\ Bd, & x > d. \end{cases} \quad (3)$$

To determine the eigenspinors $\Psi(x, y, t) = (\Psi_1, \Psi_2)^T$ in the three regions, we solve the eigenvalue equation, with T

standing for transpose. In region 2 ($0 < x < d$), we get

$$\Delta\Psi_1(x, y, t) + v_F \left[p_x - i \left(p_y - \frac{eF}{\omega} \cos(\omega t) - eBx \right) \right] \Psi_2(x, y, t) = i\hbar \frac{\partial}{\partial t} \Psi_1(x, y, t) \quad (4)$$

$$v_F \left[p_x + i \left(p_y - \frac{eF}{\omega} \cos(\omega t) - eBx \right) \right] \Psi_1(x, y, t) - \Delta\Psi_2(x, y, t) = i\hbar \frac{\partial}{\partial t} \Psi_2(x, y, t) \quad (5)$$

To proceed further, note that in the framework of the Floquet approximation [28], the oscillation of the laser field over time produces several energy modes in the eigenspinors. As a result, we have $\Psi(x, y, t) = \psi(x, y, t)e^{-\frac{iEt}{\hbar}}$ where E is the Floquet quasi-energy, $\psi(x, y, t)$ is a time periodic function satisfying $\psi(x, y, t + t_0) = \psi(x, y, t)$ and t_0 is the time period of the laser field. On the other hand, if the Hamiltonian is invariant along the y -direction, then we write $\Psi(x, y, t) = e^{ik_y y} e^{-\frac{iEt}{\hbar}} \varphi(t) (\phi_1(x), \phi_2(x))^T$, and therefore (4,5) become

$$v_F \left[-i \frac{\partial}{\partial x} - i \left(k_y - \frac{F}{\omega} \cos(\omega t) - Bx \right) \right] \phi_2(x) \varphi(t) e^{ik_y y} e^{-iEt} = \left(i \frac{\partial}{\partial t} - \Delta \right) \phi_1(x) \varphi(t) e^{ik_y y} e^{-iEt} \quad (6)$$

$$v_F \left[-i \frac{\partial}{\partial x} + i \left(k_y - \frac{F}{\omega} \cos(\omega t) - Bx \right) \right] \phi_1(x) \varphi(t) e^{ik_y y} e^{-iEt} = \left(i \frac{\partial}{\partial t} + \Delta \right) \phi_2(x) \varphi(t) e^{ik_y y} e^{-iEt} \quad (7)$$

in the system unit ($\hbar = e = c = 1$). It is straightforward to find $-i\frac{F}{\omega} \cos(\omega t) = \frac{\partial}{\partial t} \varphi(t)$ and therefore the temporal component is

$$\varphi(t) = e^{-i\alpha \sin(\omega t)}. \quad (8)$$

Now, we use the Jacobi–Anger identity $e^{-i\alpha \sin(\omega t)} = \sum_{-\infty}^{+\infty} J_m(\alpha) e^{-im\omega t}$ to write (6,7) as

$$\frac{\partial \phi_2(x)}{\partial x} - \left[\frac{x}{\ell_B^2} - k_y + m\varpi \right] \phi_2(x) - i(\varepsilon + m\varpi - \delta) \phi_1(x) = 0 \quad (9)$$

$$\frac{\partial \phi_1(x)}{\partial x} + \left[\frac{x}{\ell_B^2} - k_y + m\varpi \right] \phi_1(x) - i(\varepsilon + m\varpi + \delta) \phi_2(x) = 0 \quad (10)$$

where $\ell_B = \frac{1}{\sqrt{B}}$, $\varpi = \frac{\omega}{v_F}$, $\tilde{F} = \frac{F}{v_F}$, $\varepsilon = \frac{E}{v_F}$ and $\delta = \frac{\Delta}{v_F}$. From (9,10), we obtain two new decoupled equations

$$\frac{\partial^2 \phi_1(x)}{\partial^2 x} + \left[\frac{1}{\ell_B^2} - \left(\frac{x}{\ell_B^2} - k_y + m\varpi \right)^2 + (\varepsilon + m\varpi)^2 - \delta^2 \right] \phi_1(x) = 0 \quad (11)$$

$$\frac{\partial^2 \phi_2(x)}{\partial^2 x} + \left[-\frac{1}{\ell_B^2} - \left(\frac{x}{\ell_B^2} - k_y + m\varpi \right)^2 + (\varepsilon + m\varpi)^2 + \delta^2 \right] \phi_2(x) = 0. \quad (12)$$

These can be expressed in terms of the Weber differential equations [29, 31] by making the change of variable $X_m = \sqrt{2} \left(\frac{x}{\ell_B} - k_y \ell_B + m\varpi \ell_B \right)$ and setting $v_m = \frac{(\varepsilon \ell_B + m\varpi \ell_B)^2 - (\delta \ell_B)^2}{2}$, to get

$$\frac{d^2 \phi_{1,2}(X_m)}{dX_m^2} + \left[\pm \frac{1}{2} - \frac{X_m^2}{4} + v_m \right] \phi_{1,2}(X_m) = 0 \quad (13)$$

having the following solutions

$$\phi_1(X_m) = A_m D_{v_m}(X_m) + B_m D_{v_m}(-X_m) \quad (14)$$

$$\phi_2(X_m) = -\frac{i\sqrt{2}}{\varepsilon \ell_B + m\varpi \ell_B + \delta \ell_B} [A_m D_{v_m+1}(X_m) - B_m D_{v_m+1}(-X_m)] \quad (15)$$

where A_m, B_m are constant coefficients corresponding to m th side-band, and D_{v_m} is the parabolic cylinder function. Consequently, the eigenspinors in region 2 take the form

$$\Psi_2(x, y, t) = e^{ik_y y} \sum_{l=-\infty}^{+\infty} \left[A_l \begin{pmatrix} \Xi_l^+(x) \\ \eta_l^+(x) \end{pmatrix} + B_l \begin{pmatrix} \Xi_l^-(x) \\ \eta_l^-(x) \end{pmatrix} \right] \sum_{m=-\infty}^{+\infty} J_m(\alpha) e^{-i(\varepsilon+(l+m)\omega)t} \quad (16)$$

and we have defined

$$\Xi^\pm(x) = D_{v_m}(\pm X_m) \quad (17)$$

$$\eta^\pm(x) = \mp \frac{i\sqrt{2}}{\varepsilon\ell_B + m\varpi\ell_B + \delta\ell_B} D_{v_{m+1}}(\pm X_m). \quad (18)$$

In the region 1 ($x < 0$) we have only pristine graphene, and then we can easily obtain the associated eigenspinors and eigenvalues [18]

$$\Psi_1(x, y, t) = e^{ik_y y} \sum_{m=-\infty}^{+\infty} \left[\delta_{l,0} \begin{pmatrix} 1 \\ \Lambda_l \end{pmatrix} e^{ik_l x} + \sum_{m,l=-\infty}^{+\infty} r_l \begin{pmatrix} 1 \\ -\Lambda_l^* \end{pmatrix} e^{-ik_l x} \right] \delta_{m,l} e^{-iv_F(\varepsilon+m\varpi)t} \quad (19)$$

$$\varepsilon + l\varpi = s_l \sqrt{k_l^2 + k_y^2} \quad (20)$$

where r_l is the amplitude of the reflected wave corresponding to band l , $\delta_{m,l} = J_{m-l}(\alpha = 0)$, $s_l = \text{sgn}(v_F\varepsilon + lv_F\varpi)$, $\phi_l = \tan^{-1} \frac{k_y}{k_l}$, $k_l = \varepsilon \cos \phi_l$, $k_y = \varepsilon \sin \phi_l$ and

$$\Lambda_l = s_l \frac{k_l + ik_y}{\sqrt{k_l^2 + k_y^2}} = s_l e^{i\phi_l}. \quad (21)$$

We can establish the relation between the incident angles

$$\phi_l = \arcsin \left(\frac{\varepsilon}{\varepsilon + l\varpi} \sin(\phi_0) \right). \quad (22)$$

In region 3 ($x > d$), the emergent angle ϕ'_l is different than the incident one ϕ_0 because of the continuity of the vector potential. The solution is [18]

$$\Psi_3(x, y, t) = e^{ik_y y} \sum_{m,l=-\infty}^{+\infty} \left[t_l \begin{pmatrix} 1 \\ \Lambda'_l \end{pmatrix} e^{ik'_l x} + b_l \begin{pmatrix} 1 \\ -\Lambda'_l \end{pmatrix} e^{-ik'_l x} \right] \delta_{m,l} e^{-iv_F(\varepsilon+m\varpi)t} \quad (23)$$

$$\varepsilon + l\varpi = s_l \sqrt{k_l'^2 + \left(k_y - \frac{d}{\ell_B^2} \right)^2} \quad (24)$$

where t_l is the transmission amplitude of the transmitted wave corresponding to the band l , b_l is a null vector, $\phi'_l = \tan^{-1} \frac{k_y - \frac{d}{\ell_B^2}}{k'_l}$, $k'_l = (\varepsilon + l\varpi) \cos \phi'_l$, $k_y = (\varepsilon + l\varpi) \sin \phi'_l + \frac{d}{\ell_B^2}$ and

$$\Lambda'_l = s_l \frac{k'_l + i \left(k_y - \frac{d}{\ell_B^2} \right)}{\sqrt{k_l'^2 + \left(k_y - \frac{d}{\ell_B^2} \right)^2}} = s_l e^{i\phi'_l}. \quad (25)$$

From the conservation of the momentum k_y , we get the relation

$$\phi'_l = \arcsin \left(\frac{\varepsilon}{\varepsilon + l\varpi} \sin \phi_0 - \frac{\frac{d}{\ell_B^2}}{\varepsilon + l\varpi} \right). \quad (26)$$

As we will see, the above results can be used to study the transport properties of gapped graphene scattered by a magnetic barrier and irradiated by a laser field. We obtain the transmissions associated with several energy bands and the corresponding conductance.

III. TRANSMISSION PROBABILITIES

We use the continuity of the eigenspinors at $x = 0$ and $x = d$ to determine the transmission probabilities for the present system. This corresponds to the processes $\Psi_1(0, y, t) = \Psi_2(0, y, t)$ and $\Psi_2(d, y, t) = \Psi_3(d, y, t)$, which yields

$$\delta_{m,0} + r_m = \sum_{l=-\infty}^{+\infty} (A_l \Xi_l^+(0) + B_l \Xi_l^-(0)) J_{m-l}(\alpha) \quad (27)$$

$$\delta_{m,0} \Lambda_m - r_m \Lambda_m^* = \sum_{l=-\infty}^{+\infty} (A_l \eta_l^+(0) + B_l \eta_l^-(0)) J_{m-l}(\alpha) \quad (28)$$

$$t_m e^{ik'_m d} + b_m e^{-ik'_m d} = \sum_{l=-\infty}^{+\infty} (A_l \Xi_l^+(d) + B_l \Xi_l^-(d)) J_{m-l}(\alpha) \quad (29)$$

$$t_m \Lambda'_m e^{ik'_m d} - b_m \Lambda'_m e^{-ik'_m d} = \sum_{l=-\infty}^{+\infty} (A_l \eta_l^+(d) + B_l \eta_l^-(d)) J_{m-l}(\alpha). \quad (30)$$

We have four equations, but each one has an infinite number of modes, and to solve the problem, we use the transfer matrix approach. As a result, we get

$$\begin{pmatrix} \Upsilon_1 \\ \Upsilon'_1 \end{pmatrix} = \begin{pmatrix} \mathbb{N}_{1,1} & \mathbb{N}_{1,2} \\ \mathbb{N}_{2,1} & \mathbb{N}_{2,2} \end{pmatrix} \begin{pmatrix} \Upsilon_2 \\ \Upsilon'_2 \end{pmatrix} = \mathbb{N} \begin{pmatrix} \Upsilon_2 \\ \Upsilon'_2 \end{pmatrix} \quad (31)$$

with

$$\mathbb{N} = \begin{pmatrix} \mathbb{1} & \mathbb{0} \\ \Gamma^+ & \Gamma^- \end{pmatrix}^{-1} \begin{pmatrix} \mathbb{X}_0^+ & \mathbb{X}_0^- \\ \mathbb{R}_0^+ & \mathbb{R}_0^- \end{pmatrix} \begin{pmatrix} \mathbb{X}_d^+ & \mathbb{X}_d^- \\ \mathbb{R}_d^+ & \mathbb{R}_d^- \end{pmatrix}^{-1} \begin{pmatrix} \mathbb{1} & \mathbb{0} \\ \Gamma'^+ & \Gamma'^- \end{pmatrix} \begin{pmatrix} \mathbb{K}^+ & \mathbb{0} \\ \mathbb{0} & \mathbb{K}^- \end{pmatrix} \quad (32)$$

and

$$\Gamma^\pm = \pm \delta_{m,l} \Lambda_l^{\pm 1}, \quad \Gamma'^\pm = \pm \delta_{m,l} \Lambda_l'^{\pm 1}, \quad \mathbb{X}_z^\pm = \Xi_l^\pm(z) J_{m-l}(\alpha), \quad \mathbb{R}_z^\pm = \eta_l^\pm(z) J_{m-l}(\alpha), \quad \mathbb{K}^\pm = e^{\pm ik'_l L} \delta_{m,l} \quad (33)$$

where $\mathbb{0}$ is the zero matrix, $\mathbb{1}$ is the unit matrix and $z = \{0, d\}$. In this case, we take into account Dirac fermions traveling from left to right with energy E , and from (31), we obtain

$$\Upsilon_2 = \mathbb{N}_{1,1}^{-1} \Upsilon_1 \quad (34)$$

with the Kronecker coefficient $\delta_{0,l} = \Upsilon_1$ and $\Upsilon_2 = t_l$.

Because n and l range from $-\infty$ to $+\infty$ and are challenging to solve, the aforementioned transfer matrix is of infinite order. Due to this, we replace the infinite series with a finite set of terms ranging from $-N$ to N , provided that $N \geq \frac{F}{\omega^2}$ [18], resulting in

$$t_{-N+k} = \mathbb{N}'[k+1, N+1] \quad (35)$$

where $\mathbb{N}' = \mathbb{N}_{1,1}^{-1}$, $k = 0, 1, 2, \dots, N$. To simplify, we limit our studies only to the central band and the first two side bands $l = 0, \pm 1$ of energy $E \pm \hbar\omega$ having the following transmission coefficients

$$t_{-1} = \mathbb{N}'[1, 2], \quad t_0 = \mathbb{N}'[2, 2], \quad t_1 = \mathbb{N}'[3, 2]. \quad (36)$$

On the other hand, the current density is determined from the continuity equation, its expression given by $J = ev_F \Psi^* \sigma_x \Psi$, therefore the expression of the incident, reflected and transmitted current density given by

$$J_{\text{inc},0} = ev_F (\Lambda_0 + \Lambda_0^*) \quad (37)$$

$$J_{\text{tra},l} = ev_F t'_l t_l (\Lambda'_l + \Lambda_l^*) \quad (38)$$

$$J_{\text{ref},l} = ev_F r'_l r_l (\Lambda_l + \Lambda_l^*) \quad (39)$$

The relation between the current density and the transmission probability is expressed as $T_l = \frac{J_{\text{tra},l}}{J_{\text{inc},0}}$. Then, after some algebra, we get

$$T_l = \frac{\cos \phi'_l}{\cos \phi_0} |t_l|^2 \quad (40)$$

and the total transmission probability is given by summing up over all modes

$$T = \sum_l T_l. \quad (41)$$

By definition, the conductance at zero temperature is the average of the flux of the fermions on the half Fermi surface [32, 33], on the other hand it is the integration of the total transmission T over k_y [34], given by

$$G = \frac{G_0}{2\pi} \int_{-k_y^{\max}}^{k_y^{\max}} T dk_y \quad (42)$$

where G_0 is the conductance unit. Using the relation between transverse wave vector k_y and the incident angle ϕ_0 to express G as

$$G = \frac{G_0}{2\pi} \int_{-\frac{\pi}{2}}^{\frac{\pi}{2}} T \cos \phi_0 d\phi_0. \quad (43)$$

To investigate and underline the basic features of the present system, we numerically analyze the transport properties based on the transmission channels and associated conductance in the following chapter.

IV. RESULTS AND DISCUSSION

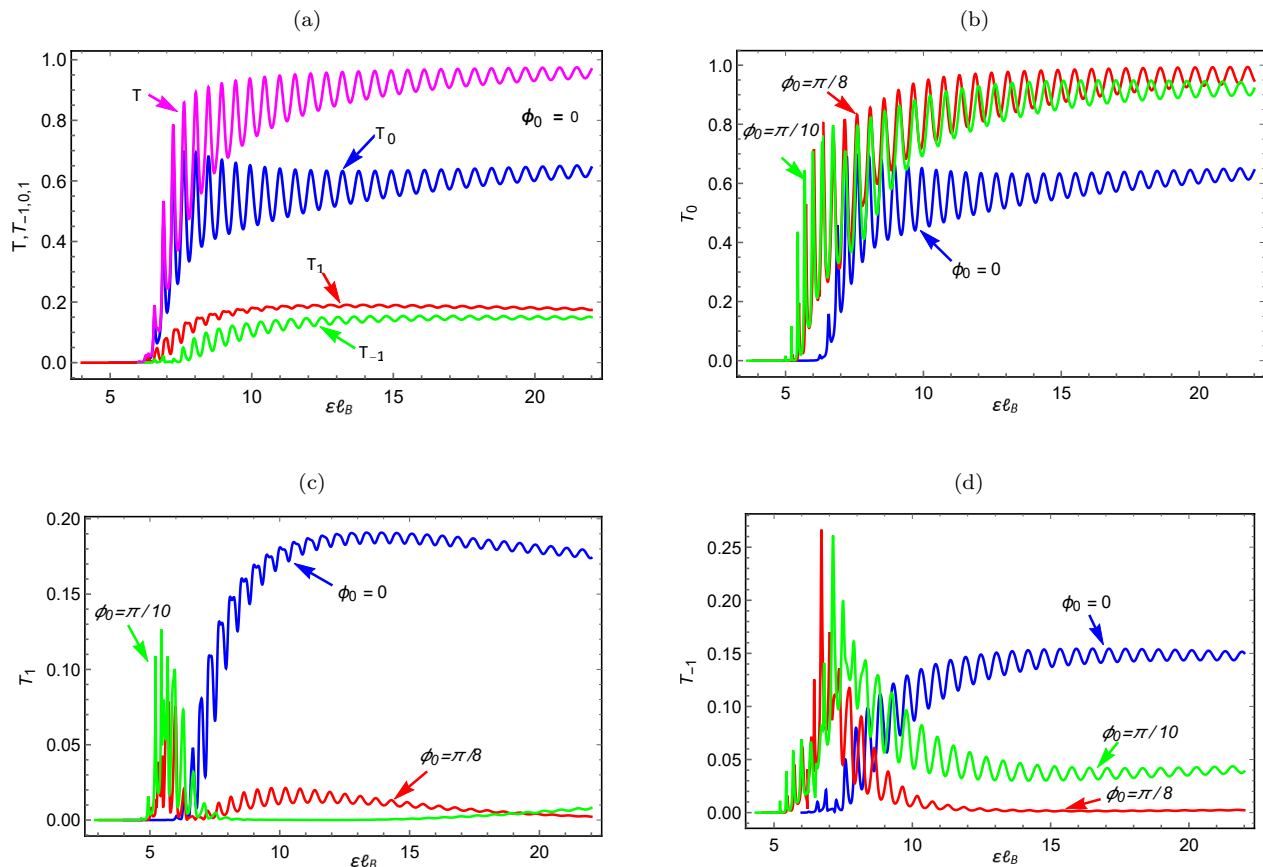


FIG. 2. (Color online) Transmission probabilities as a function of the energy $\varepsilon\ell_B$ with $\tilde{F}\ell_B^2 = 0.6$, $\varpi\ell_B = 1$, $\frac{d}{\ell_B} = 5$ and $\delta\ell_B = 5$, (a): $\phi_0 = 0$, T (magenta line) total transmission probability, T_0 (blue line), T_{-1} (green line) and T_1 (red line), (b, c, d): T_0, T_1, T_{-1} with $\phi_0 = \{0, \frac{\pi}{10}, \frac{\pi}{8}\}$.

We numerically study the transmission probabilities of Dirac fermions in gapped graphene through a magnetic barrier in a laser field. Recall that the oscillation of the barrier over time generates several energy bands, which give rise to transmission channels. Due to the difficulty of analyzing all modes, we will limit ourselves to the first three bands, where the central band T_0 corresponds to zero photon exchange and the first two side bands $T_{\pm 1}$ to absorption or emission of photons. Fig. 2 shows the transmission probability as a function of the energy $\varepsilon \ell_B$ for different incident angles. There is transmission if the condition $\varepsilon > \frac{\frac{d}{\ell_B} - l\omega}{1 + \sin \phi_0}$ is satisfied, in other words, this quantity plays the role of an effective mass [36]. For normal incidence, as depicted in Fig. 2a, transmission is zero for $\varepsilon < \delta$. Due to this condition, resonance peaks appear with decreasing amplitudes along the $\varepsilon \ell_B$ -axis, that is to say the disappearance of the Fabry-Pérot resonance, which is in agreement with previous results [23, 35]. The transmission process with zero photon exchange, T_0 , is dominating, and therefore, the majority of the electrons cross the barrier without photon exchange. Fig. 2b shows the behavior of T_0 for different incident angles, and as a result, we observe that T_0 increases sharply away from the normal incidence. On the other hand, transmission with photon exchange as shown in Figs. 2c, 2d there is a decrease for large energy. We can conclude that the behavior of T_0 changes if we move away from the normal incidence and that the photon exchange process is suppressed.

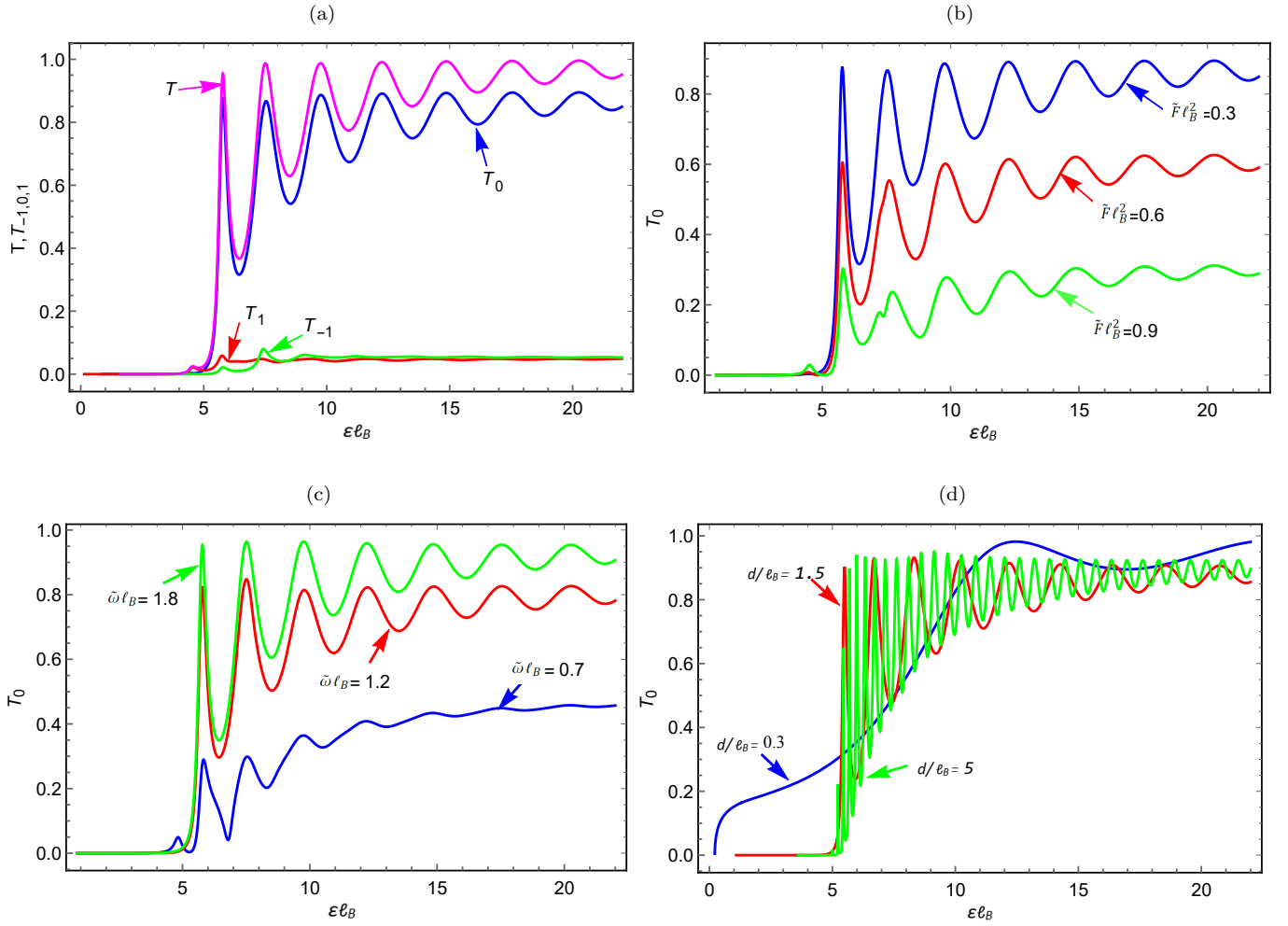


FIG. 3. (Color online) Transmission probabilities as a function of $\varepsilon \ell_B$ with $\delta \ell_B = 5$, $\phi_0 = \frac{\pi}{8}$ (a): $\tilde{F}\ell_B^2 = 0.3$, $\varpi \ell_B = 1$, $\frac{d}{\ell_B} = 1.2$, T (magenta line), T_0 (blue line), T_{-1} (green line) and T_1 (red line), (b): $\varpi \ell_B = 1$, $\frac{d}{\ell_B} = 1.2$, $\tilde{F}\ell_B^2 = \{0.3, 0.6, 0.9\}$, (c): $\frac{d}{\ell_B} = 1.2$, $\tilde{F}\ell_B^2 = 0.5$, $\varpi \ell_B = \{0.7, 1.2, 1.8\}$, (d): $\tilde{F}\ell_B^2 = 0.5$, $\varpi \ell_B = 1.5$, $\frac{d}{\ell_B} = \{0.3, 1.5, 5\}$.

Fig. 3 displays the transmission probability as a function of $\varepsilon \ell_B$ under a suitable choice of physical parameters. Transmissions appear when condition $\varepsilon > \delta$ is satisfied. As clearly seen in Fig. 3a, we observe the dominance of T_0 compared to those corresponding to the first two side bands, and it is almost equal to the total transmission as

found in [22]. Now for different values of $\tilde{F}\ell_B^2$, we plot T_0 in Fig. 3b. We see that T_0 decreases with the increase of $\tilde{F}\ell_B^2$, because the increase in laser field suppresses T_0 as we have already seen [27]. Fig. 3c displays the effect of field frequency on transmission: increasing the frequency increases T_0 . Fig. 3d is drawn for different values of barrier width $\frac{d}{\ell_B}$. If this increases, resonance peaks appear and their number increases, and the oscillations get closer. A similar result is obtained in our previous work [37].

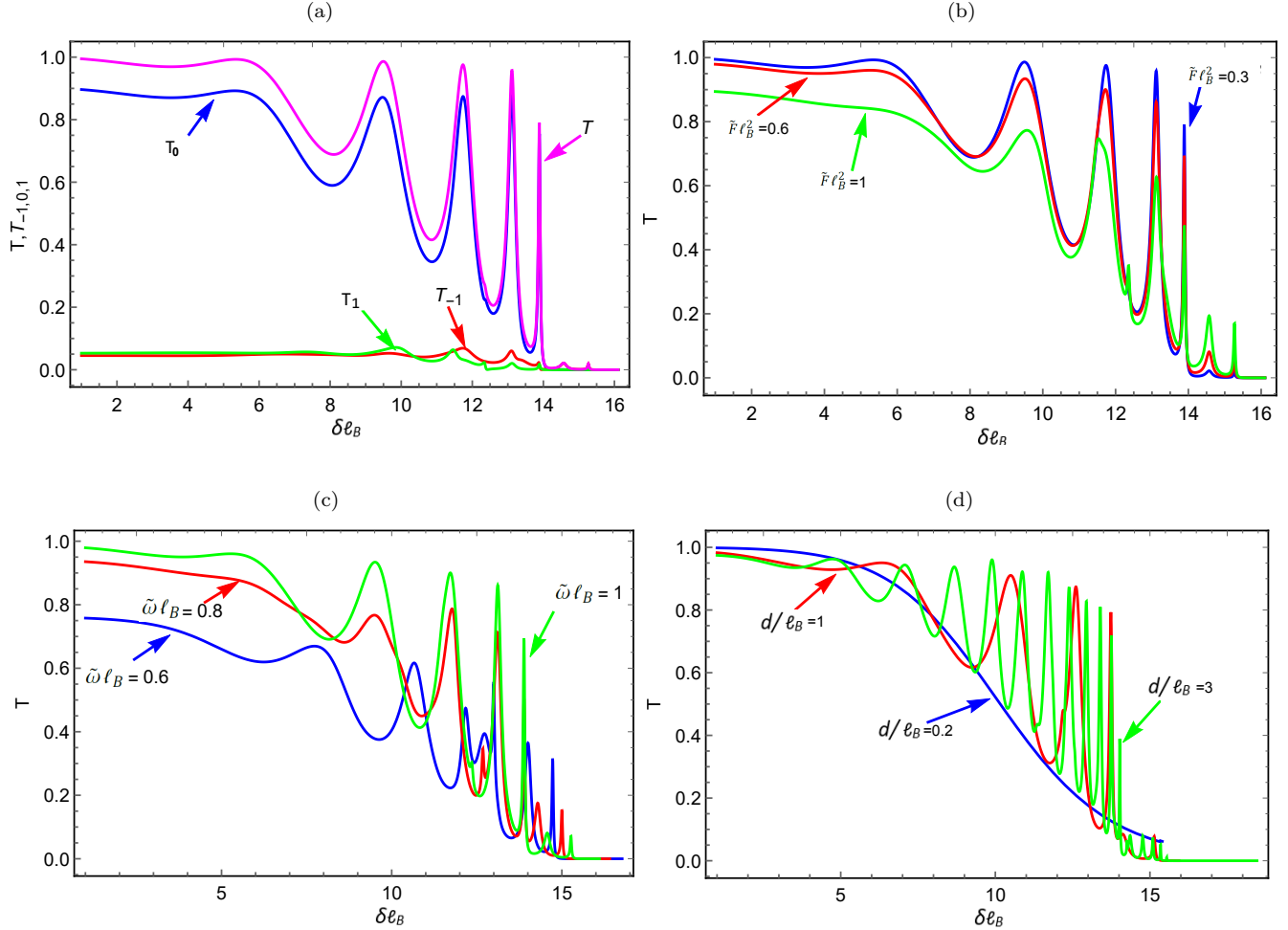


FIG. 4. (Color online) Transmission probabilities as a function of $\delta\ell_B$ with $\varepsilon\ell_B = 15$ and $\phi_0 = \frac{\pi}{8}$, (a): $\frac{d}{\ell_B} = 1.2$, $\varpi\ell_B = 1$ and $\tilde{F}\ell_B^2 = 0.3$, (b): $\frac{d}{\ell_B} = 1.2$, $\varpi\ell_B = 1$ and $\tilde{F}\ell_B^2 = \{0.3, 0.6, 1\}$, (c): $\frac{d}{\ell_B} = 1.2$, $\tilde{F}\ell_B^2 = 0.6$ and $\varpi\ell_B = \{0.6, 0.8, 1\}$, (d): $\varpi\ell_B = 1$, $\tilde{F}\ell_B^2 = 0.6$ and $\frac{d}{\ell_B} = \{0.2, 1, 3\}$.

Fig. 4 presents the transmission probabilities as a function of the energy gap $\delta\ell_B$. We show in Fig. 4a the total transmission probability (magenta line) and those with or without photon exchange. We distinguish two interesting cases: first, for $\delta\ell_B < 6$, the Klein effect is very clear and transmission with photon exchange is almost zero, that means that the majority of electrons cross the barrier without photon exchange. Second, for $\delta\ell_B > 6$, the transmissions decrease in an oscillatory way until they become zero when $\delta\ell_B$ is close to $\varepsilon\ell_B = 15$. Fig. 4b displays the total transmission for different values of $\tilde{F}\ell_B^2$, and we see that the increase of $\tilde{F}\ell_B^2$ suppresses the transmission, as has been found in [25]. The Klein effect is clear for very small values of $\tilde{F}\ell_B^2$ and $\delta\ell_B$. For $\tilde{F}\ell_B^2 = 0.3$, the Klein effect is observed only for $\delta\ell_B < 6$, then the transmission decreases in an oscillatory way until the oscillations vanish. If we increase $\tilde{F}\ell_B^2$ the transmission keeps the same shape with decreasing amplitude, which is in agreement with the results of [35]. Fig. 4c is similar to the previous one, but here we vary $\varpi\ell_B$. As a result, for $\varpi\ell_B = 1$ the Klein effect always exists up to $\varpi\ell_B = 5$, then the transmission decreases in an oscillatory way towards zero near $\varepsilon\ell_B$. On the other hand, there will be total reflection if the incident energy is lower than the energy gap. If the frequency decreases, the transmission retains the same shape, but the amplitude decreases. Fig. 4d shows the effect of the barrier width on

the total transmission. We observe that resonance peaks appear when the width increases. For very small widths, the Klein effect is found up to $\delta\ell_B \approx 6$, and then the transmission decreases towards zero. Increasing the width increases the number of oscillations and their amplitudes, as already seen in [37]. We summarize that increasing the amplitude of the field suppresses transmission inside the barrier. On the other hand, increasing the frequency increases the transmission, and increasing the width increases the number of oscillations and their amplitude.

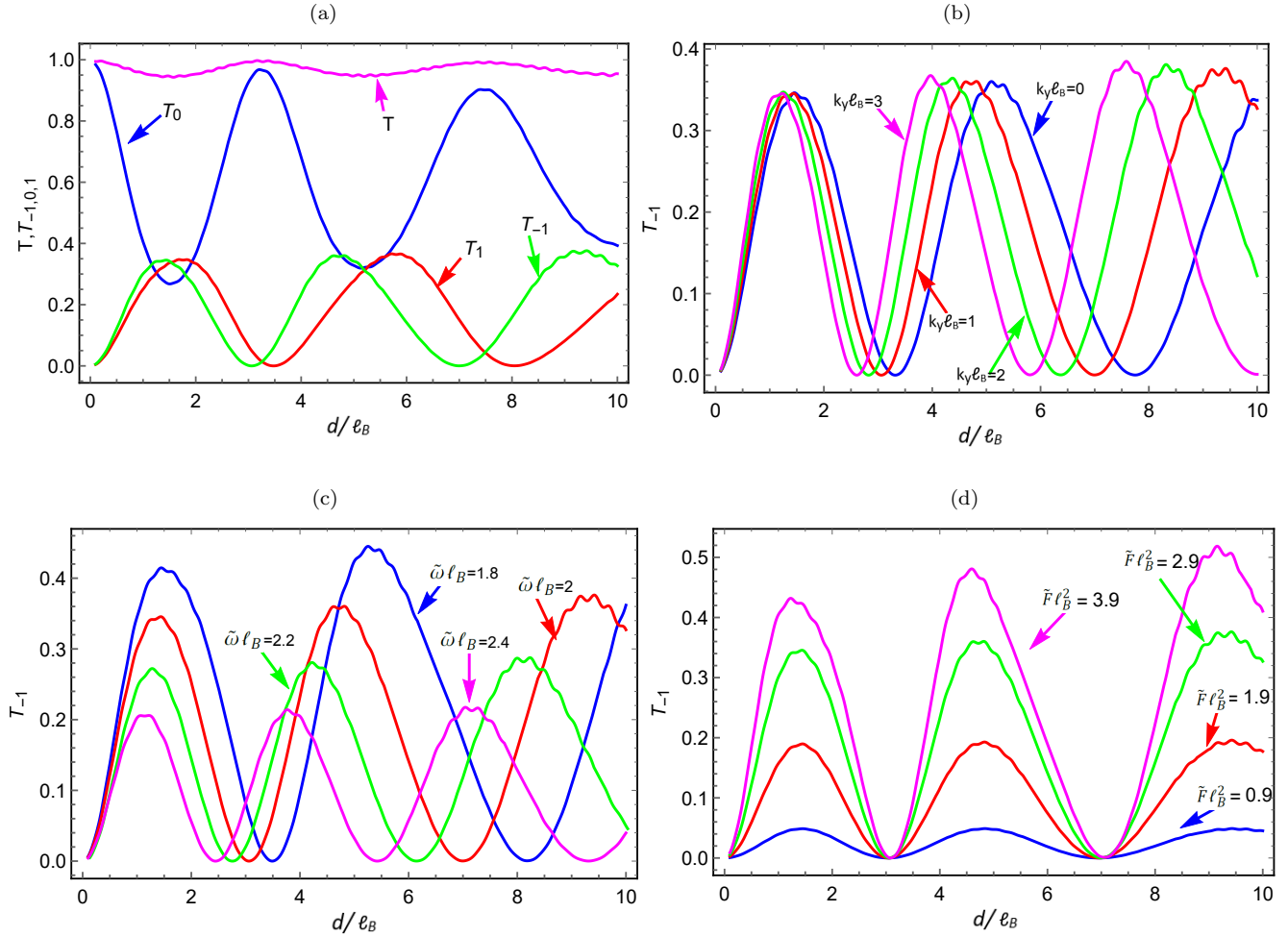


FIG. 5. (Color online) Transmission probabilities as a function of the barrier width d/ℓ_B , with $\varepsilon\ell_B = 15$ and $\Delta\ell_B = 0$, (a) $\varpi\ell_B = 2$, $k_y\ell_B = 1$, $\tilde{F}\ell_B^2 = 2.9$, (b): $\varpi\ell_B = 2$, $\tilde{F}\ell_B^2 = 2.9$ and $k_y\ell_B = \{0, 1, 2, 3\}$, (c): $k_y\ell_B = 1$, $\tilde{F}\ell_B^2 = 2.9$ and $\varpi\ell_B = \{1.8, 2, 2.2, 2.4\}$, (d): $k_y\ell_B = 1$, $\varpi\ell_B = 2$ and $\tilde{F}\ell_B^2 = \{0.9, 1.9, 2.9, 3.9\}$.

Fig. 5 shows the transmission probabilities as a function of the barrier width d/ℓ_B . In Fig. 5a we observe that all the transmissions have sinusoidal behavior. The total transmission oscillates in the vicinity of one (Klein paradox). T_0 is predominant and its oscillation amplitude decreases when the width increases. The transmissions with photon exchange also oscillate, but with phase shift, which increases along the d/ℓ_B -axis. For certain values of d/ℓ_B , the transmissions with or without photon exchange are equal. Fig. 5b displays transmission with photon emission for different values of the transverse wave vector $k_y\ell_B$. There is always a sinusoidal behavior with increasing amplitude along the d/ℓ_B -axis. When $k_y\ell_B$ increases, the width of the oscillations decreases. In Fig. 5c, we show the effect of the laser field frequency on transmission. We notice that the amplitude and period of oscillations decrease as the frequency increases. Thus, the increase in frequency suppresses the transmissions with photon exchanges. We vary the intensity of the laser field $\tilde{F}\ell_B^2$ in Fig. 5d and observe that the transmission is oscillating with the same period. We notice that the increase in $\tilde{F}\ell_B^2$ causes an increase in transmission with photon exchange and decreases that of the central band.

In Fig. 6, we plot the conductance as a function of the energy $\varepsilon\ell_B$. Choosing different values of width $\frac{d}{\ell_B}$, Fig. 6a reveals that the conductance varies almost exponentially for lower values of $\frac{d}{\ell_B}$, and oscillates when $\frac{d}{\ell_B}$ increases. Fig. 6b shows the effect of intensity $\tilde{F}\ell_B^2$ of the laser field on conductance. We observe that conductance increases as $\tilde{F}\ell_B^2$ increases, but it vanishes when $\varepsilon \rightarrow \delta$. Fig. 6c is plotted for different values of frequency $\varpi\ell_B$. We notice that the conductance tends to zero when $\varepsilon\ell_B$ is close to $\delta\ell_B$ and the oscillations increase as $\varpi\ell_B$ increases. In Fig. 6d, we vary $\delta\ell_B$ to observe that the conductance is always almost zero when ε tends towards δ . Ultimately, to enhance conductance, it is essential to augment the quantity of electrons traversing the barrier, consequently elevating transmission. As observed, transmission rises with an increase in incident energy or a reduction in barrier width, and it also climbs when the intensity of the laser field decreases or its frequency rises.

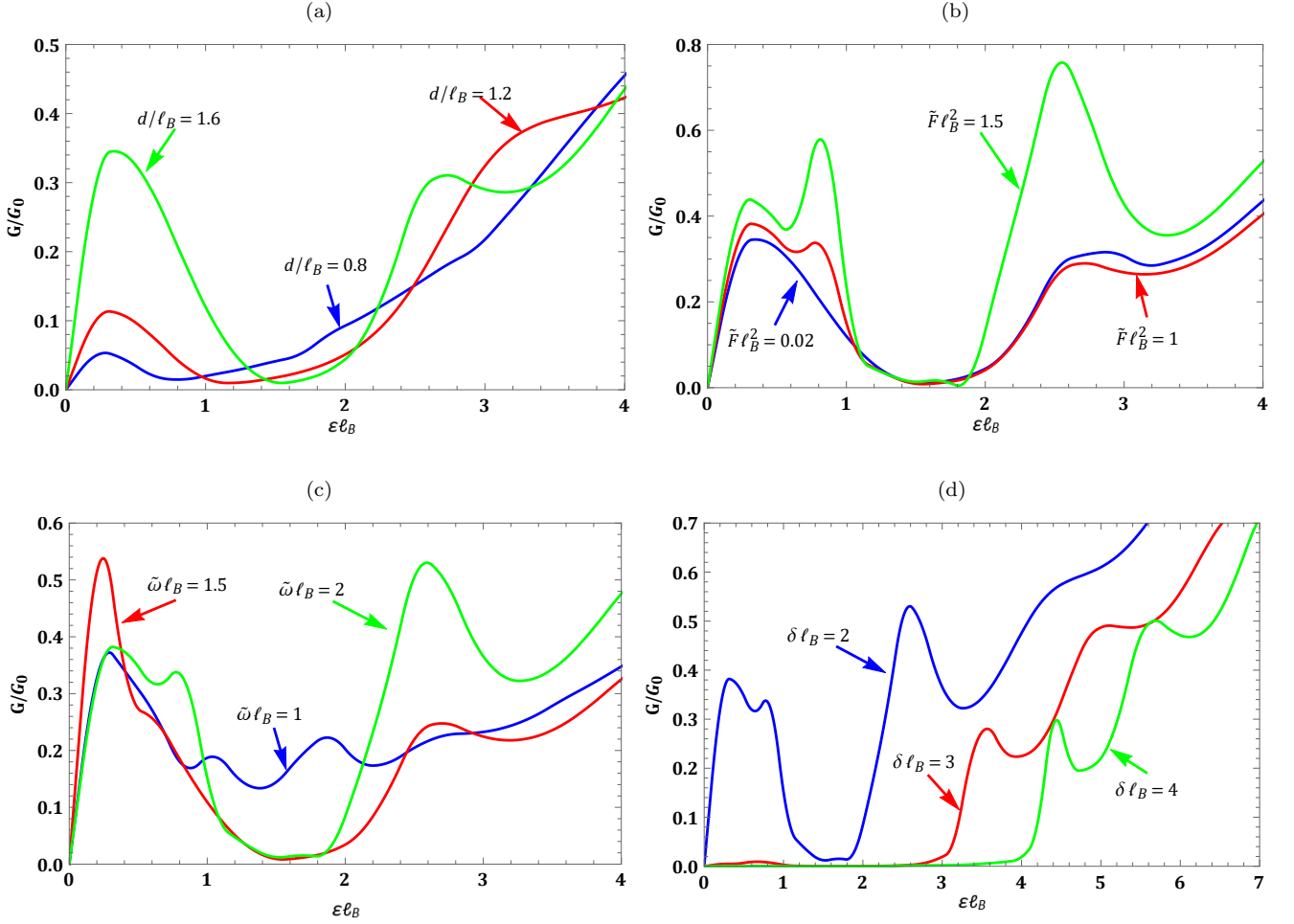


FIG. 6. (Color online) Zero temperature conductance as a function of $\varepsilon\ell_B$, (a) $\varpi\ell_B = 1$, $\tilde{F}\ell_B^2 = 0.03$, $\delta\ell_B = 2$ and $\frac{d}{\ell_B} = \{0.8, 1.2, 1.6\}$, (b): $\varpi\ell_B = 2$, $\frac{d}{\ell_B} = 1.6$, $\delta\ell_B = 2$ and $\tilde{F}\ell_B^2 = \{0.02, 1, 1.5\}$, (c): $\tilde{F}\ell_B^2 = 1$, $\frac{d}{\ell_B} = 1.6$, $\delta\ell_B = 2$ and $\varpi\ell_B = \{1, 1.5, 2\}$, (d): $\varpi\ell_B = 2$, $\frac{d}{\ell_B} = 1.6$, $\tilde{F}\ell_B^2 = 1$ and $\delta\ell_B = \{2, 3, 4\}$.

In Figure 7, the conductance is represented as a function of the energy gap $\delta\ell_B$. By choosing three values of incident energy in Fig. 7a, we show that the conductance is maximum at the beginning, then decreases in an oscillatory way towards zero near the value $\delta = \varepsilon$. The amplitude increases when incident energy increases as well, exhibiting a behavior similar to transmission as we have seen before. Fig. 7b shows the effect of width $\frac{d}{\ell_B}$ on the conductance. There are always resonance peaks that appear around $\delta\ell_B = 3$, the number of oscillations increases with the increase of $\frac{d}{\ell_B}$. In Figs. 7c and 7d, we visualize the effect of the laser field parameters on the conductance. They show that the amplitude of the conductance increases with the increase in frequency, and decreases when the amplitude increases.

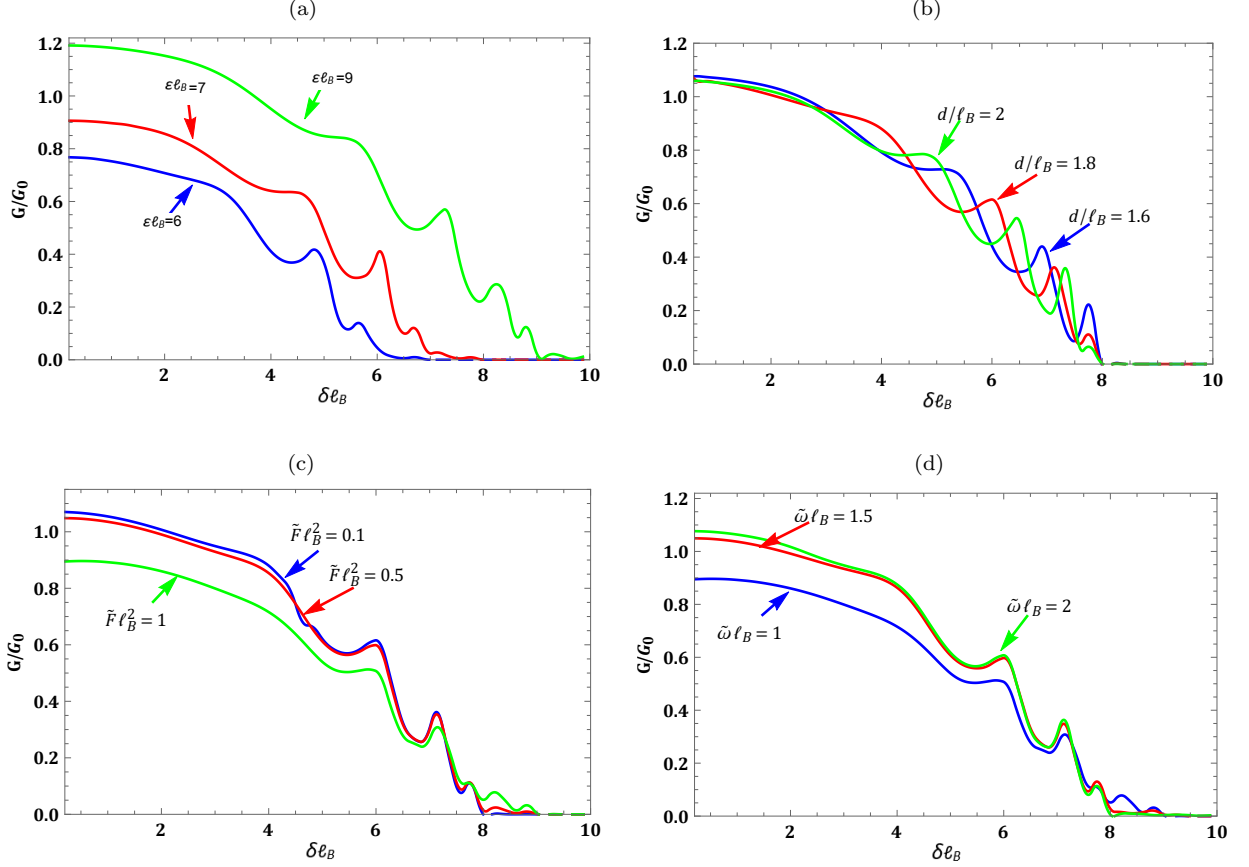


FIG. 7. (Color online) Zero temperature conductance as a function of δl_B , (a) $\varpi l_B = 1$, $\tilde{F} l_B^2 = 0.5$, $\frac{d}{l_B} = 1.8$ and $\varepsilon l_B = \{6, 7, 9\}$, (b): $\varpi l_B = 1$, $\tilde{F} l_B^2 = 0.03$, $\varepsilon l_B = 8$ and $\frac{d}{l_B} = \{1.6, 1.8, 2\}$, (c): $\varpi l_B = 1$, $\frac{d}{l_B} = 1.8$, $\varepsilon l_B = 8$ and $\tilde{F} l_B^2 = \{0.1, 0.5, 1\}$, (d): $\tilde{F} l_B^2 = 1$, $\frac{d}{l_B} = 1.8$, $\varepsilon l_B = 8$ and $\varpi l_B = \{1, 1.5, 2\}$.

V. CONCLUSION

We studied the effect of a gapped magnetic barrier irradiated by a laser field generated by an electric field of amplitude F and frequency ω on Dirac fermions in graphene. We started with the solution of the eigenvalue equations to determine the spinors in the three regions of the gapped sheet. We used the Floquet theory, and the solution of Weber's differential equation to determine the eigenspinors corresponding to each region as combinations of parabolic cylindrical functions. Then we employed the boundary conditions, which give four equations, each equation has infinite modes. To solve them, we used the transfer matrix approach to obtain a matrix of infinite order that is difficult to solve. For simplicity, we focused only on the three first bands, the central band corresponds to $l = 0$ and the two first side bands correspond to $l = \pm 1$. Lastly, we calculated the integral of the total transmission probability to obtain conduction at zero temperature.

When a barrier oscillates in time, it generates several energy bands, namely the photon exchange between the barrier and the Dirac fermions. Here we found that the transmission process with zero photon exchange is much more important than the process with photon exchange. Klein's paradox is still present, but we can suppress it. As we know, the original Klein effect is only observed for normal incidences ($\phi_0 = 0$), but in this work, this effect is observed for non-normal incidences. When the barrier width is increased, the transmission decreases until it disappears for a critical width, the same thing happens for the conductance. On the other hand, the transmission increases when the incident energy increases. However, to have transmission, it is necessary to satisfy the condition that binds the incident energy to the other barrier parameters: $\varepsilon > \frac{\frac{d}{l_B} - l\varpi}{1 + \sin \phi_0}$. As we know the conductance exists if we have a non-zero

transmission, which always implies the verification of this last condition..

-
- [1] K. S. Novoselov, A. K. Geim, S. V. Morozov, D. Jiang, Y. Zhang, S. V. Dubonos, I. V. Grigorieva, and A. A. Firsov, *Science* 306, 666 (2004).
 - [2] K. S. Novoselov, A. K. Geim, S. V. Morozov, D. Jiang, M. I. Katsnelson, I. V. Grigorieva, S. V. Dubonos, and A. A. Firsov, *Nature* 438, 197 (2005).
 - [3] S. Morozov, K. Novoselov, M. Katsnelson, F. Schedin, D. Elias, J. Jaszczak, and A. Geim, *Phys. Rev. Lett.* 100, 016602 (2008).
 - [4] K. I. Bolotin, K. J. Sikes, Z. Jiang, M. Klima, G. Fudenberg, J. Hone, P. Kim, and H. L. Stormer, *Solid State Commun.* 146, 351 (2008).
 - [5] C. Lee, X. Wei, J. W. Kysar, and J. Hone, *Science* 321, 385 (2008).
 - [6] C. W. Beenakker, *Rev. Mod. Phys.* 80, 1337 (2008).
 - [7] S. Bhattacharjee and K. Sengupta, *Phys. Rev. Lett.* 97, 217001 (2006).
 - [8] J. S. Bunch, Y. Yaish, M. Brink, K. Bolotin, and P. L. McEuen, *Nano Lett.* 5, 2887 (2005).
 - [9] C. Berger, Z. M. Song, T. B. Li, X. B. Li, A. Y. Ogbazghi, R. Feng, Z. T. Dai, A. N. Marchenkov, E. H. Conrad, P. N. First, and W. A. de Heer, *J. Phys. Chem. B* 108, 19912 (2004).
 - [10] S. Reich, J. Maultzsch, C. Thomsen, and P. Ordejon, *Phys. Rev. B* 66, 035412 (2002).
 - [11] A. H. Castro Neto, F. Guinea, N. M. R. Peres, K. S. Novoselov, and A. K. Geim, *Rev. Mod. Phys.* 81, 109 (2009).
 - [12] N. M. R. Peres, *J. Phys.: Condens. Matter* 21, 323201 (2009).
 - [13] F. Guinea, M. I. Katsnelson, and A. K. Geim, *Nat. Phys.* 6, 30 (2010).
 - [14] G.-X. Ni, Y. Zheng, S. Bae, H. R. Kim, A. Pachoud, Y. S. Kim, C.-L. Tan, D. Im, J.-H. Ahn, B. H. Hong, and B. Ozyilmaz, *ACS Nano* 6, 1158 (2012).
 - [15] S. Latil and L. Henrard, *Phys. Rev. Lett.* 97, 036803 (2006).
 - [16] S. V. Morozov, K. S. Novoselov, F. Schedin, D. Jiang, A. A. Firsov, and A. K. Geim, *Phys. Rev. B* 72, 201401 (2005).
 - [17] M. I. Katsnelson, K. S. Novoselov, and A. K. Geim, *Nat. Phys.* 2, 620 (2006).
 - [18] A. Jellal, M. Mekkaoui, E. B. Choubabi, and H. Bahlouli, *Eur. Phys. J. B* 87, 123 (2014).
 - [19] A. De Martino, L. Dell'Anna, and R. Egger, *Phys. Rev. Lett.* 98, 066802 (2007).
 - [20] F. Xu and L. Zhang, *Chin. Phys. B* 28, 117403 (2019).
 - [21] M. O. Goerbig, *Rev. Mod. Phys.* 83, 1193 (2011).
 - [22] N. Myoung and G. Ihm, *Physica E* 42, 70 (2009).
 - [23] R. El Aitouni and A. Jellal, *Phys. Lett. A* 447, 128288 (2022).
 - [24] R. Biswas and C. Sinha, *Appl. Phys.* 114, 183706 (2013).
 - [25] C. Sinha and R. Biswas, *Appl. Phys. Lett.* 100, 183107 (2012).
 - [26] M. Ahsan Zeb, K. Sabeeh, and M. Tahir, *Phys. Rev. B* 78, 165420 (2008).
 - [27] R. El Aitouni, M. Mekkaoui, A. Jellal, *Ann. Phys. (Berlin)* 535, 2200630 (2023).
 - [28] Z. Gu, H. A. Fertig, D. P. Arovas, and A. Auerbach, *Phys. Rev. Lett.* 107, 216601 (2011).
 - [29] I. S. Gradshteyn, I. M. Ryzhik, *Table of Integrals, Series, and Products* (Academic Press, Inc. New York, 1980).
 - [30] R. Loudon, *The Quantum Theory of Light* (3rd ed, Oxford University Press, New York, 2000).
 - [31] F. W. J. Olver, *J. Res. Nat. Bur. Standards Sect. B* 63, 131 (1959).
 - [32] X. Chen and J. W. Tao, *Appl. Phys. Lett.* 94, 262102 (2009).
 - [33] M. R. Masir, P. Vasilopoulos, and F. M. Peeters, *Phys. Rev. B* 79, 035409 (2009).
 - [34] R. Biswas and C. Sinha, *Sci. Rep.* 11, 2881 (2021).
 - [35] M. Mekkaoui, R. El Kinani, and A. Jellal, *Mater. Res. Expr.* 6, 085013 (2019).
 - [36] M. Mekkaoui, A. Jellal, and H. Bahlouli, *Solid State Communi.* 358, 114981 (2022).
 - [37] H. Chnafa, M. Mekkaoui, A. Jellal, and A. Bahaoui, *Physica E* 148, 115645 (2023).